Cretaceous Research 66 (2016) 115–128

Contents lists available at ScienceDirect

Cretaceous Research

journal homepage: www.elsevier.com/locate/CretRes

Paleoceanographic evolution and chronostratigraphy of the Aptian Oceanic Anoxic Event 1a (OAE1a) to oceanic red bed 1 (ORB1) in the Gorgo a Cerbara section (central Italy)

Juan Li, Xiumian Hu*, Kuidong Zhao, Yuanfeng Cai, Tao Sun

State Key Laboratory of Mineral Deposit Research, School of Earth Sciences and Engineering, Nanjing University, Nanjing 210023, China

ARTICLE INFO

Article history:
Received 1 June 2015
Received in revised form
15 March 2016
Accepted in revised form 29 April 2016
Available online 12 May 2016

Keywords:
Oceanic Anoxic Event 1a
Oceanic red bed 1
Aptian
Gorgo a Cerbara
Cretaceous
Italy

ABSTRACT

We performed a detailed study of the stratigraphic transition of Oceanic Anoxic Event 1a (OAE1a) to oceanic red bed 1 (ORB1) from the classic Gorgo a Cerbara section in the Umbria region of central Italy. We focused on a 25.5-m-thick stratigraphic succession, from which we analyzed 305 samples for total organic carbon (TOC), $CaCO_3$, magnetic susceptibility, diffuse reflectance spectrophotometry and the stable carbon and oxygen isotopic composition of both bulk samples and organic matter. In the Gorgo a Cerbara section, the Selli Level of OAE1a (~1.81 m thick) consists of laminated to bioturbated dark gray to black mudstones and shales with medium to dark gray radiolarian-rich silty to sandy layers and a maximum TOC content of 20.22%. The carbon isotopic values show a negative excursion (C3 stage, ~0.14 m) at the base of the Selli Level, followed by a stepwise positive excursion (C4–C6 stages, ~1.67 m) in the upper part of the Selli Level. The transition from OAE1a to ORB1 (~3.19 m thick) is characterized by bioturbated greenish gray cherty limestones and marly limestones with subordinate marls, corresponding to stable carbon isotopic C7 stage and lasts for ~0.75 Ma. The ORB1 interval (~13.15 m) consists of reddish marly claystones, dark-red marlstones, red marly limestones and red calcareous shales which indicate a highly oxic environment. Our results reveal a stepwise transition from a predominantly mesotrophic and dysoxic to anoxic environment at the time that the OAE1a black shales were deposited to an oligotrophic and oxic environment during the transitional interval and finally to highly oxic conditions during the ORB1 interval. The nannoconid crisis occurs at the top of the C2 stage, just 0.34 m below the negative excursion in $\delta^{13}C$ isotopic values. The massive $CaCO_3$ dissolution phase occurs 0.25 m above the negative excursion; it persisted for 0.85 Ma and probably resulted from excess CO_2, ocean acidification, and carbonate compensation depth (CCD) shoaling. Deposition of massive black shales occurs at the base of the C6 stage and lasted for 0.4 Ma.

1. Introduction

The early Aptian was marked by major perturbations in the global carbon cycle associated with considerable environmental change (Leckie et al., 2002; Jenkyns, 2003; Wagreich et al., 2011). These perturbations are expressed by positive excursions in the $\delta^{13}C$ values of both carbonates and organic carbon, and they may be coeval with the widespread deposition of laminated organic-rich sediments that represent oceanic anoxic events (OAEs; Schlanger and Jenkyns, 1976). The early Aptian includes one of the most significant and intensively studied of these events, OAE1a, which is also called the "Selli Event" (Arthur et al., 1990; Erba, 1994; Menegatti et al., 1998; Mehay et al., 2009; Tejada et al., 2009; Erba et al., 2010). Geologic evidence suggests that OAE1a was characterized by the deposition of organic-rich sediments in pelagic basins, extreme greenhouse conditions (Dumitrescu et al., 2006), increases in continental weathering and runoff (Najarro et al., 2011), and a negative excursion in the carbon isotopic values of carbonate and organic carbon material, followed by a pronounced positive excursion (Menegatti et al., 1998). Further, OAE1a is coeval with significant sea-level rise and a major change in nannofossil assemblages (Erba, 1994; Menegatti et al., 1998), which may indicate a period of ocean acidification (Erba et al., 2010). The mechanism that triggered OAE1a is thought to be a phase of intense

* Corresponding author. Tel.: +86 25 89683002.
E-mail address: huxm@nju.edu.cn (X. Hu).

http://dx.doi.org/10.1016/j.cretres.2016.04.016
0195-6671/

volcanism that included the emplacement of the Ontong-Java Plateau, a large igneous province (LIP; Weissert and Erba, 2004; Mehay et al., 2009; Tejada et al., 2009).

Most previous studies have examined the OAE1a black shales or the record preceding OAE1a (Kuhnt et al., 2011; Stein et al., 2011 and references therein). Less attention has focused on the changes after OAE1a, with the exception of studies of the Yenicesihlar section in central Turkey. Oceanic red beds (ORBs) were formed in the Tethyan Ocean during the late Aptian shortly after OAE1a (Hu et al., 2006, 2012; Wang et al., 2011). To date, the environmental changes associated with the transition between the OAE1a black shales and the ORBs have not been well documented (Patruno et al., 2015). To better understand the paleoenvironmental changes during the transition from OAE1a to the first reddish limestones of ORB1 (Hu et al., 2006), this study examines a classic pelagic stratigraphic section in central Italy and compares it to the Yenicesihlar section.

2. Geologic setting

The Cretaceous pelagic sequence of the Umbria-Marche Basin was deposited near the northern edge of a "promontory" of the African plate (the "Adria continental microplate"; Satolli et al., 2007; Patruno et al., 2015). The basement of the Umbria-Marche Apennines is continental, with Upper Jurassic to lower Miocene pelagic strata overlying a Triassic to Lower Jurassic carbonate platform. During the latest phase of the Alpine-Himalayan orogeny during the Miocene (Centamore et al., 2002), the basin was involved in tectonic compression and became part of the Alpine-Apennine orogen.

The Lower Cretaceous sedimentary succession that crops out in the Umbria-Marche Basin has been subdivided into two discrete formations based on color changes, carbonate content and the presence or absence of chert and black shales: the Maiolica (upper Tithonian-lower Aptian) and Marne a Fucoidi (lower Aptian-upper Albian) formations. The Maiolica Formation consists primarily of whitish to medium-gray pelagic limestones; near the top of the formation, these include beige to black chert nodules to layers and dark-gray to black, organic-rich horizons with variable carbonate content. The overlying Marne a Fucoidi Formation is a more shale-rich sequence of dark-gray to black calcareous shales, light-green-gray marly limestones containing intervals of interbedded red and green marlstones, as well as calcareous mudstones.

3. Stratigraphy and sedimentary petrology

The Gorgo a Cerbara section is located in the Umbria Marche Basin in the northern Apennines of central Italy, 4 km east of the town of Piobbico along the Candigliano River (Fig. 1). It is a key reference section for the Tethyan domain, and the proposed GSSP stratotype for the Barremian/Aptian boundary (Channell et al., 2000; Gradstein et al., 2012). There is detailed and integrated magnetostratigraphy, chemostratigraphy and cyclostratigraphy for the entire section (Herbert et al., 1995; Channell et al., 2000; Speranza et al., 2005; Tejada et al., 2009; Stein et al., 2011). In addition, a calcareous nannofossil and planktic foraminiferal biostratigraphic framework has been established, along with ammonites, calpionellids, palynomorph and radiolarians (Coccioni et al., 1992; Erba, 1994; Coccioni et al., 2006; Coccioni et al., 2012; Patruno et al., 2015; Unida and Patruno, 2015).

The measured section is approximately 25.5 m thick, and the sequence encompasses the transition between the Maiolica and Marne a Fucoidi formations, as well as between OAE1a and ORB1. Detailed descriptions of the section's lithostratigraphy can be found in Patruno et al. (2015) and Unida and Patruno (2015) (Fig. 2). The uppermost part of the Maiolica can be divided into lithozones I and II, which consist of rhythmic alternations of white-grayish medium pelagic limestones with black clay layers, greenish-gray marly limestones and dark cherts (Fig. 3a). The lowermost part of the Marne a Fucoidi can be divided into seven lithozones (lithozones III–IX) according to Patruno et al. (2015). Lithozone III is the lowermost part of the Marne a Fucoidi and is characterized by whitish pelagic limestone. Subsequently, the Lower Transition Interval of lithozone IV is 0.26 m (Patruno et al., 2015) or 0.34 m thick (this study) and is dominated by white-grayish cherty limestones. Lithozone V (the Selli Level) is 1.81 m thick and consists of black or dark-gray shales intercalated with gray marlstones and silty-sandy beds (Fig. 3b); the black shales lie within the *Leupoldina cabri* planktic foraminiferal biozone (early Aptian) and have been correlated to OAE1a (Patruno et al., 2015). Lithozones VI and VII are 3.19 m thick and include greenish-gray bioturbated limestones with very thinly bedded gray calcareous marls or shales. In some areas, centimeter-thick brownish-gray, parallel-laminated, silty limestones occur; these may be calci-turbidites (Fig. 3c). Lithozone VIII mainly consists of reddish marly claystones; lithozone IX is dominated by bioturbated dark-red marlstones, red marly limestones and red calcareous shales with subordinate gray marlstones and marly limestones that occur in beds from 1 to 30 cm thick (Fig. 3d). The reddish lithozones VIII-IX are assumed to be equivalent to the late Aptian ORB1 (Hu et al., 2006).

4. Analytical methods

This section was described at the centimeter scale in the field. A total of 305 samples were collected for laboratory analysis at a resolution of 10–20 cm. We follow the lithozones proposed by Patruno et al. (2015), setting meter 0 to correspond with the top of the highest Maiolica-like bed, which is thick and whitish (Bed A). However, we use our own thickness measurements.

4.1. Total organic carbon (TOC)

Samples for TOC analysis were first treated with 10% HCl at 60 °C to remove carbonate, then washed with distilled water to remove HCl. Next, the samples were dried overnight at 50 °C and measured using a LECOCS-200 carbon-sulfur instrument at the Wuxi Research Institute of Petroleum Geology at SINOPEC, China. The standard deviation of the TOC measurements is lower than ±0.10%.

4.2. Calcium carbonate

Calcium carbonate analyses were performed on 83 bulk rock samples that were powdered from polished surfaces using a dental drill. The calcium carbonate content was measured using an NFP18-508 calcimeter at the State Key Laboratory of Marine Geology of Tongji University, China. The method measures the CO_2 volume produced by the complete dissolution of pre-weighed samples (100 ± 1 mg each) in 10% vol. HCl. The total carbonate content (wt.% $CaCO_3$) was computed with a precision of 1% using formulas that take into account the pressure and temperature of the laboratory, the amount of bulk sample used, and the volume of CO_2 evolved in the calcimeter. Pure calcium carbonate standards were measured every ten samples to ensure proper calibration.

4.3. Bulk stable carbon and oxygen isotopic compositions

The carbon and oxygen stable isotopic compositions of 253 whole rock samples were determined using a Finnigan MAT Delta

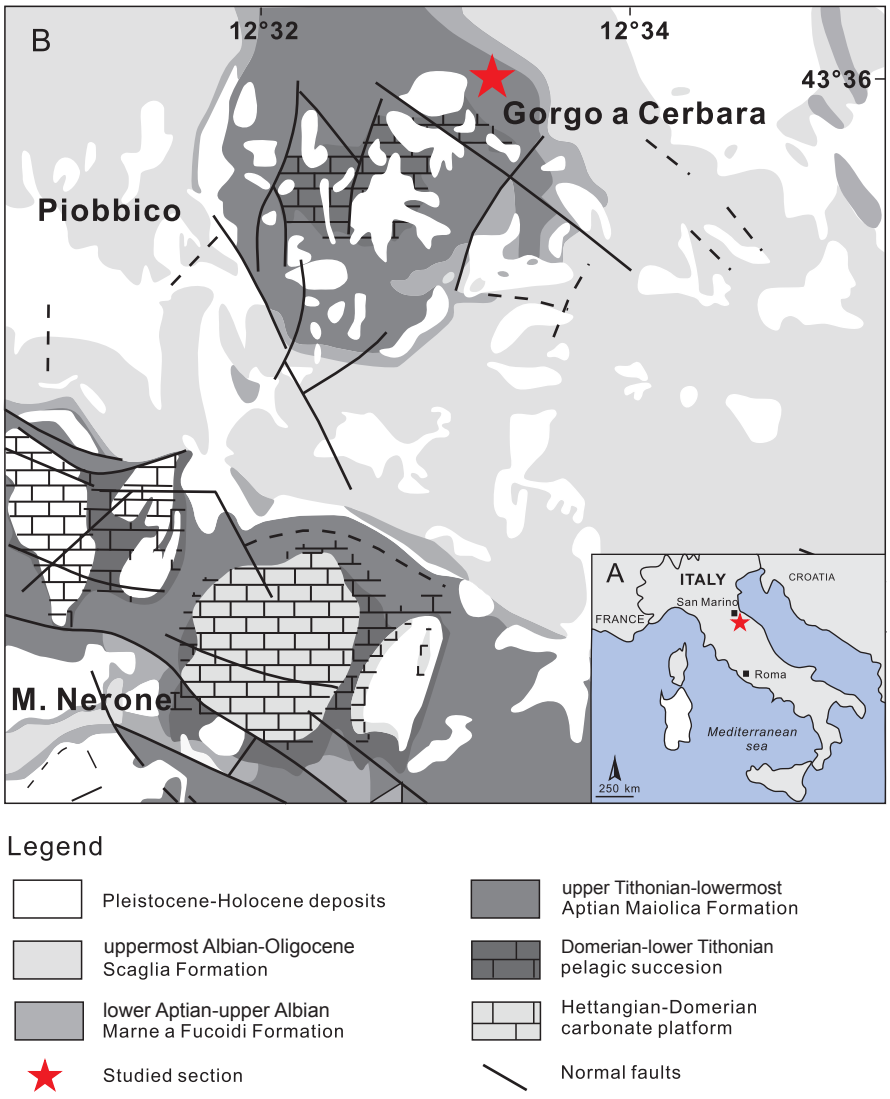

Fig. 1. A) Location of the Gorgo a Cerbara section; B) Schematic geographic map of the Gorgo a Cerbara-Mount Nerone seamount area, after Patruno et al. (2015).

Plus XP mass spectrometer equipped with an automated carbonate reaction device (Gasbench II) at the State Key Laboratory for Mineral Deposits Research of Nanjing University, China. Samples were initially reacted with purified orthophosphoric acid at 70 °C and then analyzed in-line using the mass spectrometer. The results are expressed as permil deviations relative to the PeeDee belemnite (PDB) standard. Duplicate measurements of working standards yielded identical values within the limits of analytical precision (1σ): 0.05‰ for $\delta^{13}C$ and 0.07‰ for $\delta^{18}O$.

4.4. Organic stable carbon isotopic composition

The stable isotopic composition of the organic carbon fractions of samples was also determined. The samples were decalcified with 10% HCl and analyzed using a Finnigan MAT Delta Plus XL, C003 mass spectrometer at the Wuxi Research Institute of Petroleum Geology of SINOPEC, China. The results are reported relative to PDB with a standard error of <0.05.

4.5. Diffuse reflectance spectrophotometry (DRS)

Sixteen samples from the Gorgo a Cerbara section were analyzed with DRS, following the procedures described in Ji et al. (2002). Samples were ground to <38 μm, after which the powder was suspended in distilled water to produce a slurry on a glass microslide. This slurry was smoothed, dried slowly at low temperature (<40 °C), and analyzed with a Perkin-Elmer Lambda 6 spectrophotometer equipped with a diffuse reflectance attachment (a reflectance sphere) that scanned from 400 to 2500 nm at the Institute of Surficial Geochemistry of Nanjing University. Data processing was restricted to the visible range (400–700 nm). The data are reported as percent reflectance relative to the Spectralon standard. First derivative values (percent per nanometer) were calculated at 10 nm intervals to enhance the variability of the reflectance data.

4.6. Magnetic susceptibility

A total of 302 samples were collected at approximately 2-cm intervals using non-magnetic 8.0 cm^3 plastic cubes for magnetic susceptibility analysis. Each plastic cube was gently pushed into sediments with the arrow at the bottom of the plastic cube pointing up-section, after which it was carefully removed to avoid disturbance. Analyses were performed using a Kappa bridge KLY-3 susceptibility meter at the State Key Laboratory for Mineral Deposits Research of Nanjing University, China.

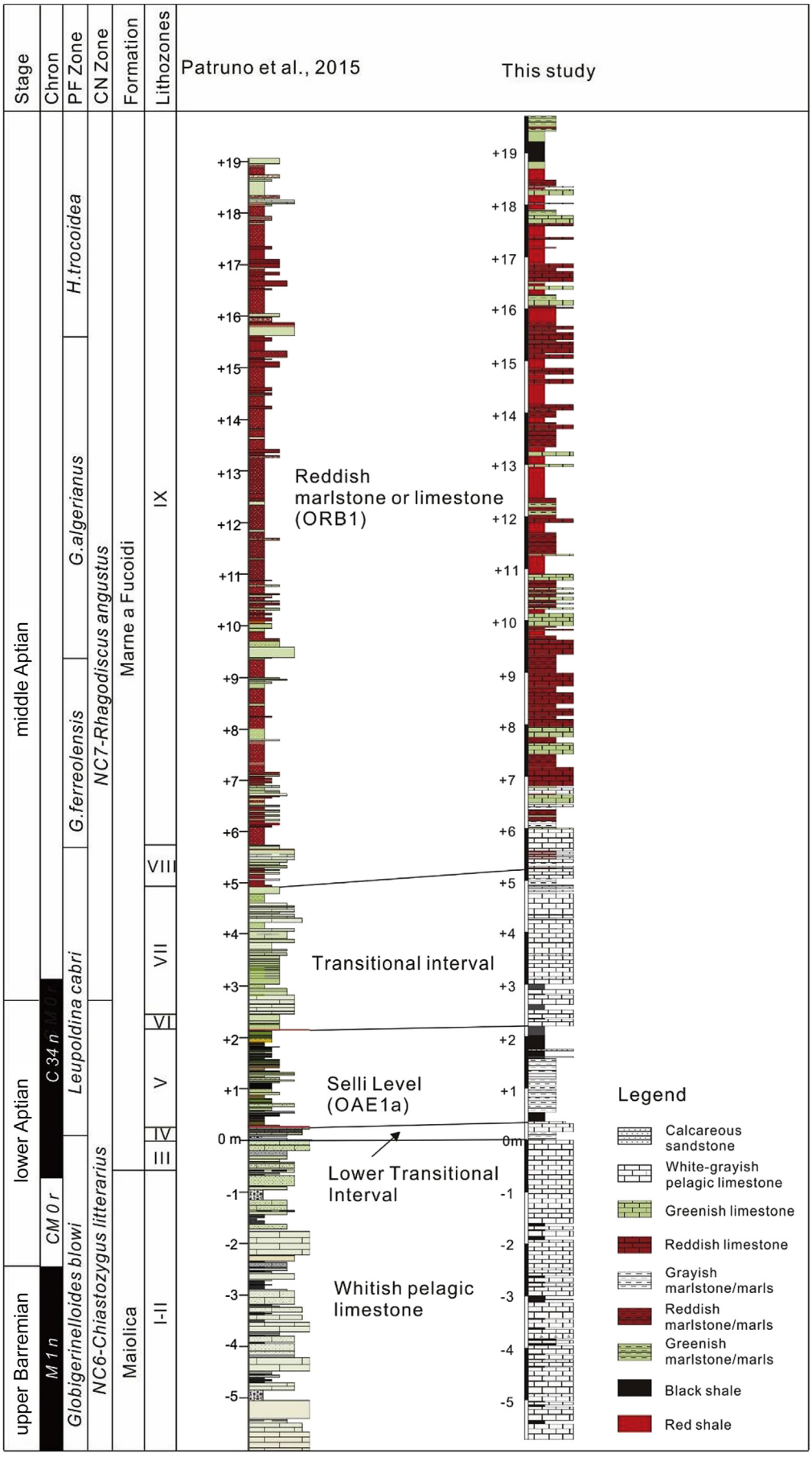

Fig. 2. Stratigraphic position of major litho-and bio-horizons in the Gorgo a Cerbara section according to the stratigraphic measurements of this study and Patruno et al. (2015). PF indicates planktic foraminifera and CN indicates calcareous nannofossils.

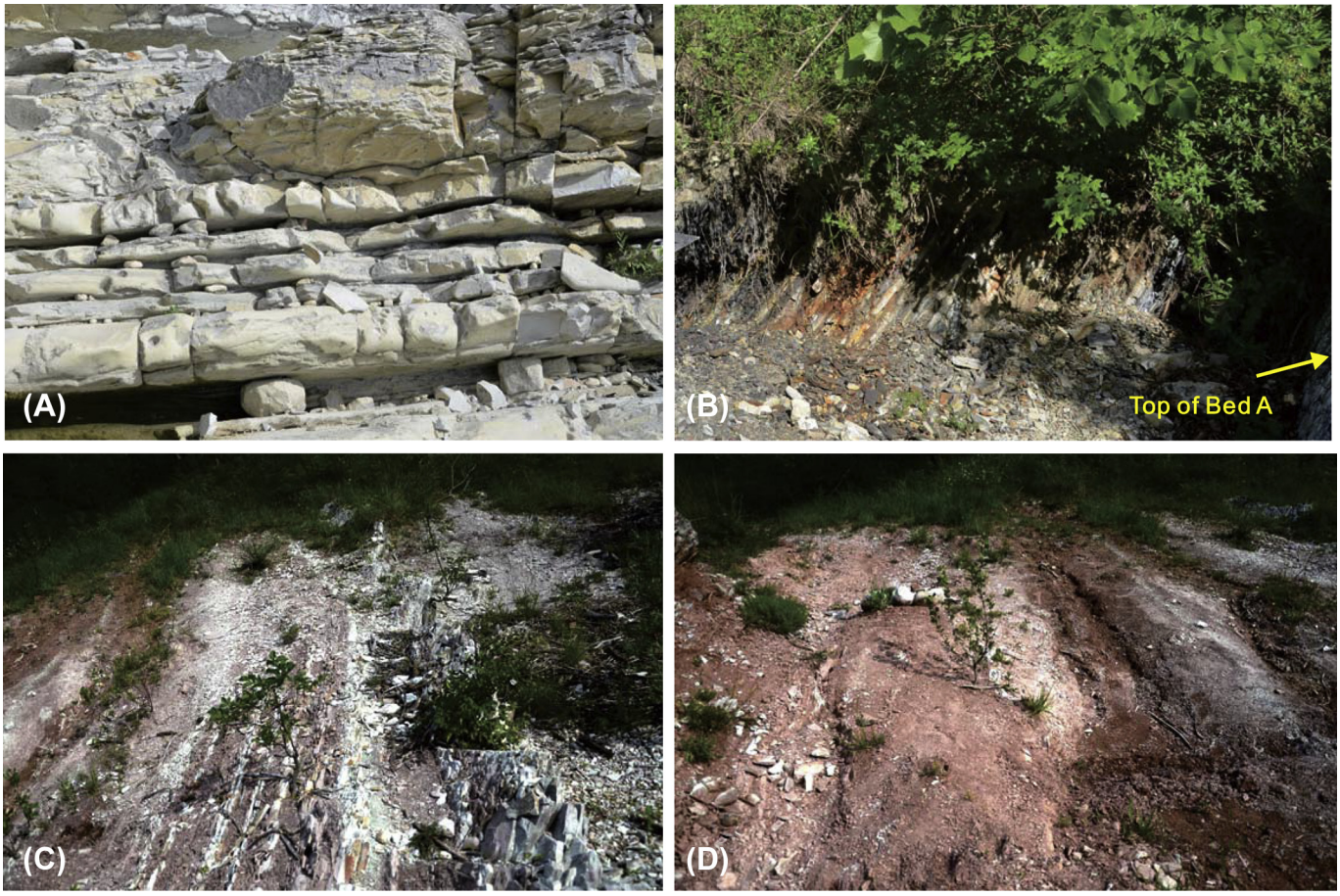

Fig. 3. Field photos in the Gorgo a Cerbara section. A). Whitish pelagic limestone and the darker interval in the upper part of the Maiolica Formation; B). The Selli Level interval; C) The transition interval between the Selli Level and ORB1; D) Red marly sediments representing the lower part of ORB1.

5. Results

5.1. Total organic carbon

The TOC values of the gray limestones from lithozones IV and III (n = 5) are extremely low, with values ranging from 0.01 to 0.02% (Fig. 4). In total, 15 samples were analyzed for TOC from lithozone V, the Selli Level (Fig. 4). The TOC values of this lithozone's dark-gray marls and black shales range from <1.00% to 20.22%; the maximum values occur in the upper part of the Selli Level. The TOC values of the gray limestones from lithozones VI and IX are very low, ranging from 0.01 to 0.05% (n = 72) (Fig. 4).

5.2. $CaCO_3$ content

The $CaCO_3$ content of the gray limestones from lithozone IV ranges from 38.0 to 62.0%. The $CaCO_3$ content abruptly decreases from 51.7% in the uppermost part of the lithozone IV to 23.1% in the base of the Selli Level. The samples from the Selli Level are virtually devoid of carbonate except for the basal part of the Selli Level and some upper layers, from which values range between 10.2 to 59.0% and 4.0 to 16.7%, respectively. In the uppermost part of the Selli Level, the $CaCO_3$ content increases abruptly from 4.0 to 46.8%, after which it varies between 41.9 and 75.6% with an average $CaCO_3$ value of 51.9% in lithozones VI to VII (Fig. 4).

5.3. Stable carbon and oxygen isotopic values

The carbon stable isotopic values ($\delta^{13}C_{carb}$) of whole rocks can be used to divide the sequence into nine stages (C1–C9, Fig. 5), following the classification of Menegatti et al. (1998). Through out most of the C1 stage, the $\delta^{13}C_{carb}$ values remain relatively stable, varying from 2.0 to 2.7‰. In the uppermost part of stage C1, however, the $\delta^{13}C_{carb}$ values gradually increase, reaching a maximum of 3.0‰ at the top of lithozone III (Bed A). The $\delta^{13}C_{carb}$ values then decrease gradually to 2.43‰ during the C2 stage. At the base of the Selli Level, which is equivalent to the C3 stage, $\delta^{13}C_{carb}$ values abruptly fall to 1.0‰ which may, at least in part, be a reflection of the relatively limited number of samples suitable for $\delta^{13}C_{carb}$ analysis. During the C4 stage, the $\delta^{13}C_{carb}$ values undergo a step-like positive shift from 1.4 to 1.8‰ (Fig. 4 and 5). During the C5 stage, the $\delta^{13}C_{carb}$ values remain between 1.6 and 1.8‰. There is a second abrupt increase from 1.0‰ to 4.31‰ during the C6 stage. During the C7 stage, which is regarded as a carbon isotopic plateau, the $\delta^{13}C_{carb}$ values range from 3.55 to 4.64‰ with an average value of 4.28‰. Subsequently, the $\delta^{13}C_{carb}$ values gradually decrease from 3.85‰ to 2.47‰ during stage C8, and, during stage C9, they slowly increase from 2.5 to 3.9‰ which are higher than before the excursion (Fig. 5).

The organic carbon isotopic values ($\delta^{13}C_{org}$) of whole rocks can also be used to divide the sequence into five stages (C3–C8, Fig. 4). These data can help illuminate the carbonate-poor intervals of stages C3–C6, which have few $\delta^{13}C_{carb}$ data. At the base of the Selli Level, the $\delta^{13}C_{org}$ value falls sharply to −28.8‰ (Fig. 4).

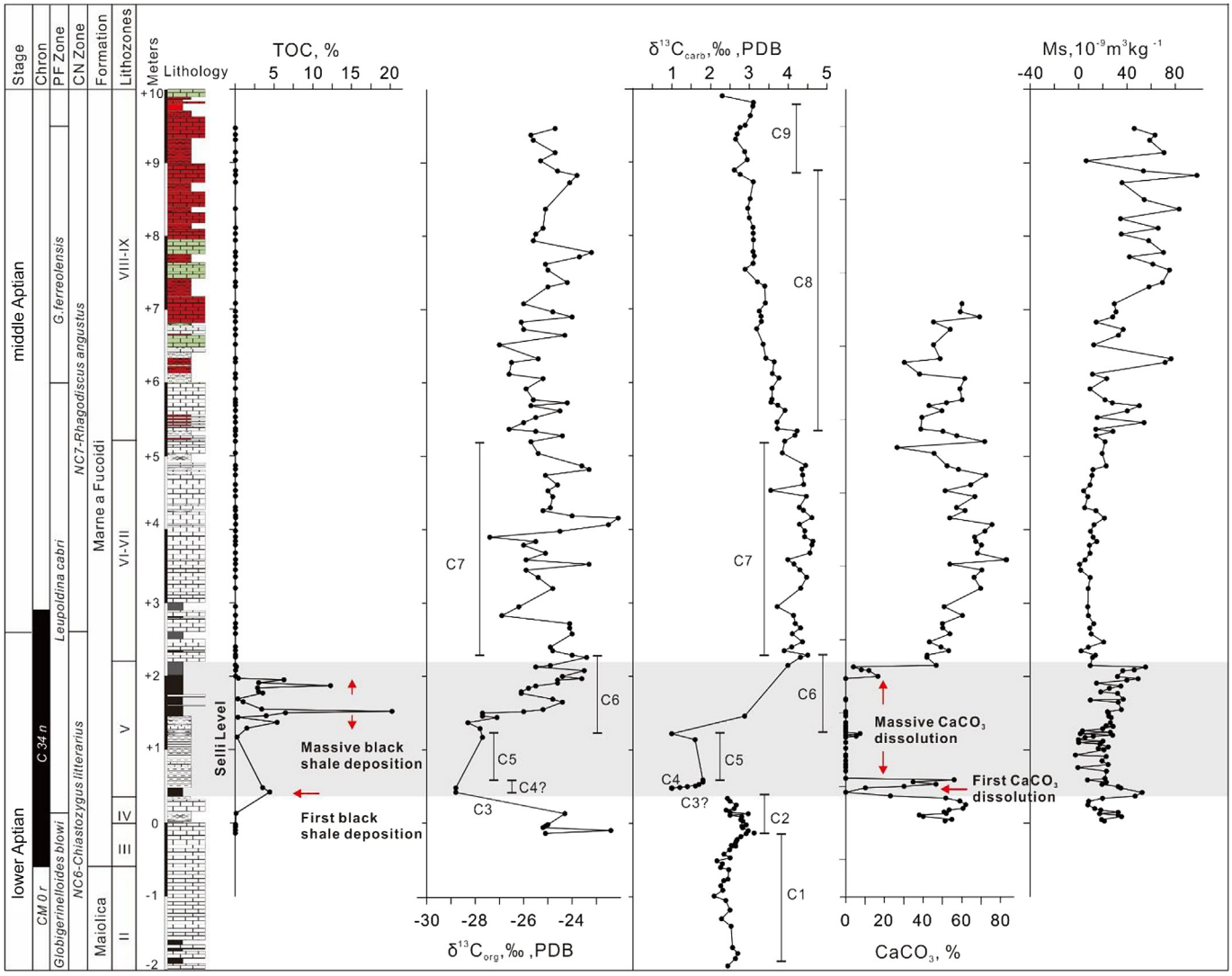

Fig. 4. Geochemical results, including TOC, $CaCO_3$, magnetic susceptibility, and carbon stable isotopic values of both bulk and organic matter near OAE1a in the Gorgo a Cerbara section.

Subsequently, the $\delta^{13}C_{org}$ values vary consistently between −28.8 and −27.7‰ during the C4 and C5 stages. Subsequently, as with the $\delta^{13}C_{carb}$ values, the $\delta^{13}C_{org}$ values exhibit an abrupt increase from −27.8 to −24.9‰ during the C6 stage in the upper part of the Selli Level. During the C7 stage, the $\delta^{13}C$ values are relatively stable, varying from −22.5 to −26.2‰. The structure and trend of the $\delta^{13}C_{org}$ values is generally similar to the $\delta^{13}C_{carb}$ values. However, during the C8 stage, the $\delta^{13}C_{carb}$ values gradually decrease, while the $\delta^{13}C_{org}$ values remain stable between stages C7 and C8.

In contrast to the $\delta^{18}C$ values, the $\delta^{18}O$ values exhibit more variation throughout the section, ranging from −4.2 to −1.3‰ (Fig. 5). The $\delta^{18}O$ values are −1.48 to −3.53‰ below the Selli Level and decrease up-section (Fig. 5). After OAE1a, the $\delta^{18}O$ values are variable, though they generally increase (Fig. 5). These trends are also apparent in strata from Cismon, in northern Italy; from Sicily, in southern Italy (Bellanca et al., 2002); from La Bédoule in south eastern France (Herrle et al., 2004; Kuhnt et al., 2011); and from Yenicesihlar, in central Turkey (Hu et al., 2012).

5.4. Magnetic susceptibility (χ)

Magnetic susceptibility (χ) data for the section are shown in Fig. 5. From lithozones I to III, χ values were generally low, varying between -7.89×10^{-9} and 4.99×10^{-9} m^3/kg, with an average value of 0 m^3/kg. At the bottom of lithozone IV, χ first increases and then decreases; it reaches a maximum of 35.54×10^{-9} m^3/kg that corresponds to the C2 stage. During the C3 stage, χ values increase abruptly at the base of the Selli Level to a maximum of 52.51×10^{-9} m^3/kg. Within the Selli Level, χ values first decrease abruptly to 22.96×10^{-9} m^3/kg during the C4 stage; during the C5 stage, they vary between 16.24×10^{-9} and 28.56×10^{-9} m^3/kg. At the top of the Selli Level, corresponding to stage C6, χ values gradually increase to a value of 55.34×10^{-9} m^3/kg. After this, χ values decrease abruptly during the C7 stage and lithozones VI and VII, varying between 0.86×10^{-9} and 22.81×10^{-9} m^3/kg. The C8 stage is characterized by a gradual increase in χ values and during the C9 stage, they decrease to values ranging from 10.29×10^{-8} to 9.74×10^{-9} m^3/kg in lithozones VIII and IX. In general, the trend in χ values is similar to the trend in $\delta^{13}C_{carb}$ values (Fig. 5).

The carbonate content and magnetic susceptibility values of the sediment are inversely correlated ($r^2 = -0.64$, Fig. 6), which confirms that the magnetic susceptibility primarily reflects the clay content of most sediments (Martinez et al., 2012; Ghirardi et al., 2014). However, the magnetic susceptibility is probably also influenced by the presence of pyrite in the Gorgo a Cerbara samples.

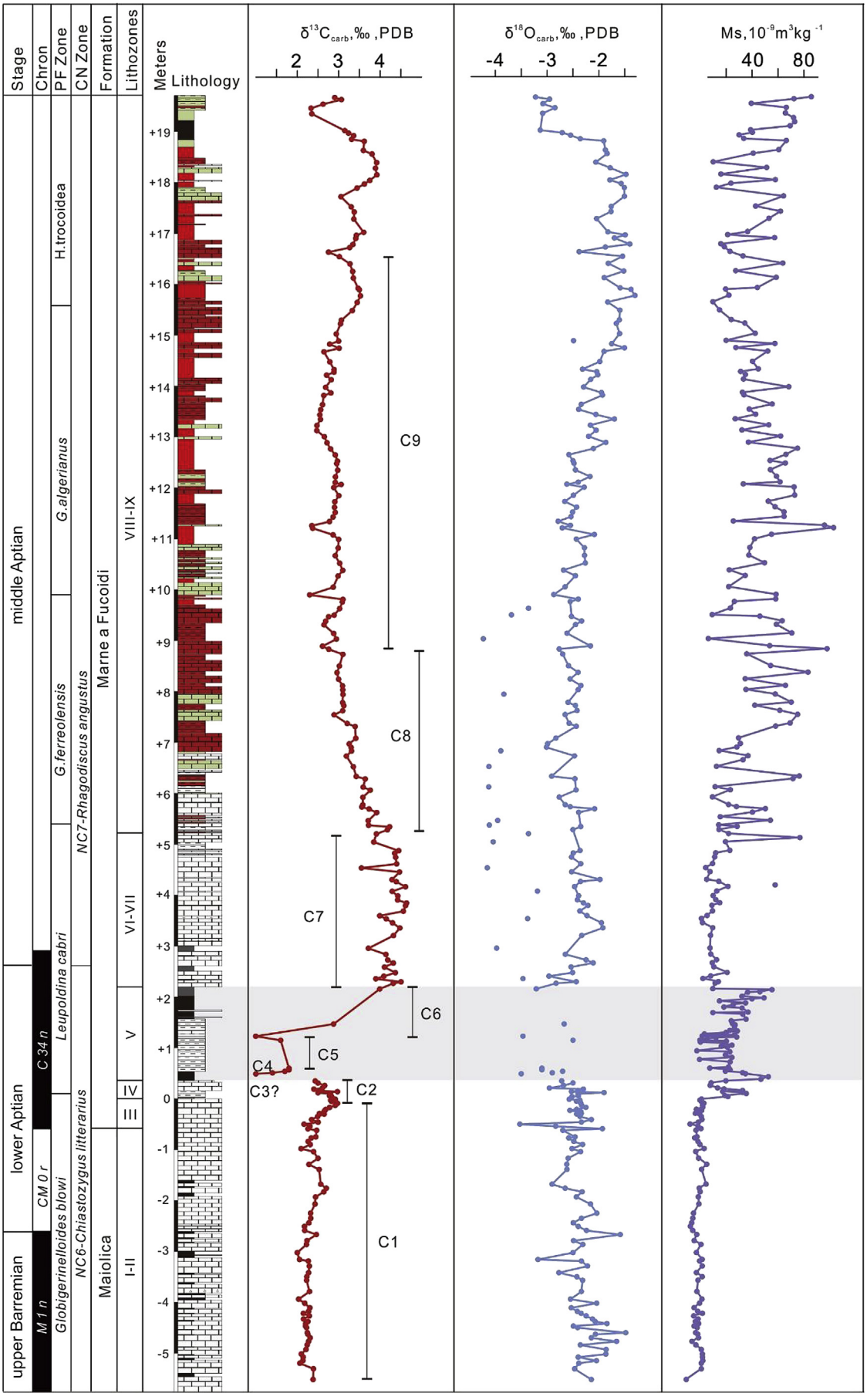

Fig. 5. Geochemical profiles of magnetic susceptibility and stable isotopic values of the measured Gorgo a Cerbara stratigraphic section. The planktic foraminiferal zones are taken from Patruno et al. (2015). The determination of bulk-rock $\delta^{13}C$ stages follows Menegatti et al. (1998).

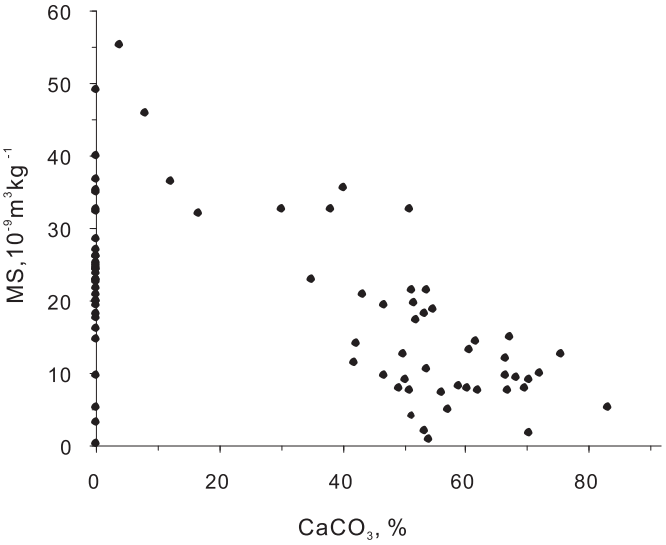

Fig. 6. Plot of $CaCO_3$ content versus magnetic susceptibility in the Gorgo a Cerbara section.

5.5. Diffuse reflectance spectrophotometry

Hematite and goethite can be easily identified from the first derivative curves of the DRS data (Deaton and Balsam, 1991). Hematite is associated with a single prominent peak at either 565 or 575 nm. Goethite has two first derivative peaks, including a primary peak at 535 nm and a secondary peak at 435 nm (Deaton and Balsam, 1991). The heights of the hematite and goethite peaks increase with the content ratios of these minerals (Deaton and Balsam, 1991). The DRS data shows that the dark-red marly limestones from lithozones VIII–IX in the Gorgo a Cerbara section contain hematite; there is a single prominent peak between 560 nm in the first derivative curves (Fig. 7). The curves of ORB1 are very similar to those from reddish limestones in Gubbio, Italy (Hu et al., 2009) and Yenicesihlar (Turkey, Hu et al., 2012). There are no peaks in the DRS data for samples from the light-gray limestones from lithozones VI–VII and the black shales from lithozone V in the Gorgo a Cerbara section. This lack of peaks suggests that these strata do not have hematite or goethite (Fig. 7).

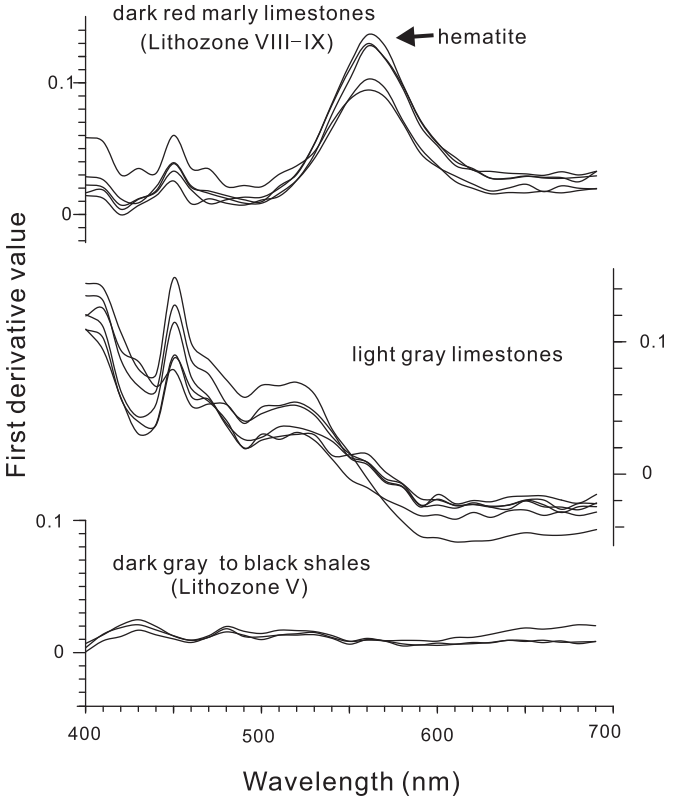

Fig. 7. First derivatives from the diffuse reflectance spectrometry (DRS) analyses for the dark red marly limestones (upper), light gray limestones (middle) and dark-gray to black shales (lower) from the Gorgo a Cerbara section. Note the peak at approximately 565 nm in the red marly limestones, which represents hematite.

6. Discussion

6.1. Paleoenvironmental changes from OAE1a to ORB1

Our field observations and lithofacies analyses provide insight into the paleoenvironmental evolution of the Gorgo a Cerbara section from OAE1a to ORB1 during the Aptian. The pre-OAE1a interval includes lithozones II to IV and is characterized by the rhythmic alternation initially between oligotrophic conditions and oxygenated water with k-selected nannoconids and *Rhizammina* followed by temporarily dysoxic condition with dominant radiolarians in lithozone I, after that there is a decrease in nannoconids and an increase in micropaleontological taxa indicative increasing eutrophy in lithozones II to IV (Patruno et al., 2015). There was no coarse siliciclastic input from terrestrial sources, as evidenced by low and stable magnetic susceptibility values (Fig. 5). The abundance presence of benthic and planktic foraminifera, as well as low TOC and χ values indicates low organic carbon flux and high dissolved oxygen levels.

OAE1a (lithozone V, the Selli Level) is virtually devoid of carbonate, as evidenced by its $CaCO_3$ content (Fig. 4). The lack of benthic foraminifera indicates an anoxic environment (Patruno et al., 2015). Barren calcareous plankton assemblages together with abundant radiolarians, resulted in TOC values that fluctuate between 0.33% and 20.22%; this is consistent with the results of Baudin et al. (1998), Menegatti et al. (1998), Danelian et al. (2002) and Stein et al. (2011). These environmental conditions may have resulted from the proximal volcanic phase of the Ontong-Java Plateau, as documented by very low $^{187}Os/^{188}Os$ ratios (Tejada et al., 2009; Bottini et al., 2012). Together, the high organic carbon content and magnetic susceptibility values, the low carbonate content and the lack of benthic foraminifera within the black shales of OAE1a indicate an anoxic environment.

The transitional interval that separates the Selli Level and ORB1 includes lithozones VI and VII. An increase in the abundance and diversity of both planktic foraminifera and nannofossils takes places in this interval, together with a return of nannoconids (Coccioni et al., 1992; Patruno et al., 2015). Similarly, benthic foraminiferal levels recover and the assemblage diversifies throughout this interval, while radiolarians decline. The abundance and diversity of planktic microfossils, nannofossils and benthic foraminifera, together with low TOC values, higher carbonate content and low magnetic susceptibility values suggest a shift from anoxic conditions to eutrophic and dysoxic conditions during this interval.

The ORB1 interval includes lithozones VIII to IX. During this interval, both planktic and benthic foraminiferal assemblages are dominated by well-developed, large and calcareous species (Patruno et al., 2015), which indicate eutrophic and well-oxygenated conditions. The reddish limestones have peaks characteristic of hematite (Fig. 7), which is similar to the reddish limestone Sogukcam facies in Turkey. This facies also has hematite peaks and has been interpreted as an oxic environment (Hu et al.,

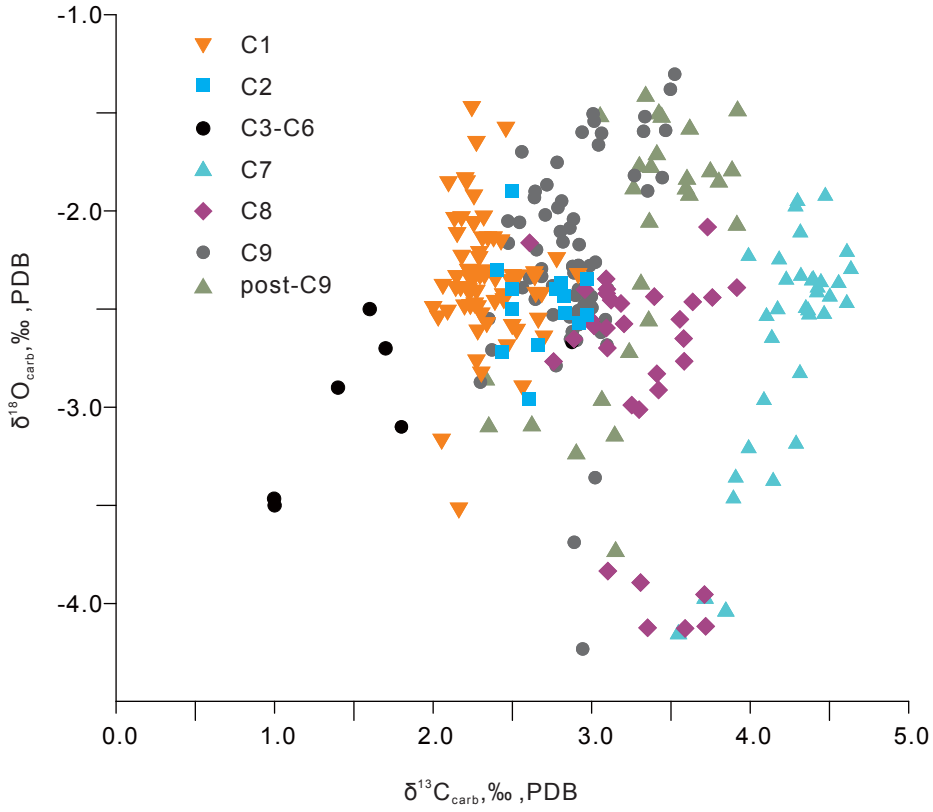

Fig. 8. Plot of measured bulk rock carbon versus oxygen stable isotopic values ($\delta^{13}C_{carb}$ vs. $\delta^{18}O_{carb}$) in the Gorgo a Cerbara section.

2012) because of authigenic nano-grains formed under oxic conditions at the same time the red limestones were deposited (Cai et al., 2012).

In Gorgo a Cerbara section, lithological variations and shifts in planktic and benthic organisms reveal a stepwise transition from a predominantly oligotrophic and oxic environment (pre-OAE1a, in the late Barremian) to an increasingly mesotrophic and dysoxic to anoxic environment (duringOAE1a, in the early Aptian) and back to oligotrophic and oxic conditions (post OAE1a, during the late "middle Aptian" and ORB1).

6.2. Carbon isotopic values and the OAE1a-ORB1 transition

A cross-plot of $\delta^{13}C_{carb}$ values and $\delta^{18}O$ values does not show a correlation between the oxygen and carbon isotopic values ($r^2 = 0.000027$; Fig. 8). Furthermore, the plot does not show the pronounced slope characteristic of a "mixing line" produced by the addition of variable quantities of isotopically homogeneous cement to isotopically homogeneous skeletal calcite (Marshall, 1992). Most of the $\delta^{13}C_{carb}$ values fall between 1.0 and 4.6‰, and most of the $\delta^{18}O$ values range from −4.2 to −1.3‰ (Fig. 8). These are comparable to records from contemporaneous basins elsewhere in the Tethyan realm (Weissert and Erba, 2004; Föllmi et al., 2006). This isotopic signature may be considered to be a record of primary paleoceanographic information.

The chronostratigraphic framework established for the Gorgo a Cerbara section by Patruno et al. (2015) was used to infer the duration of carbon isotope stages C1 to C9 (Table 1). Using the timescale of Malinverno et al. (2012), Patruno et al. (2015) assigned an age of 120.76 Ma and a duration of 1.11 Ma to the onset a duration of 1.11 Ma to the OAE1a, respectively. The carbon isotopic record can be subdivided into three distinct stages from the bottom of OAE1a to the bottom of ORB1. These include a negative excursion during C3 (0.14 m), a positive excursion during C4 to C6 (1.67 m) and an isotopic plateau during C7 (3.19 m) (Figs. 4 and 5).

Many studies have shown that OAE1a is characterized by a pronounced negative carbon isotope excursion preceding the increase in $\delta^{13}C$ values. The negative $\delta^{13}C$ excursion occurs at 0.34 m just below the base of the Selli Level in the Gorgo a Cerbara section. Taking 1.11 Ma as the mean duration of OAE1a (Malinverno et al., 2012), the excursion lasted for 0.09 Ma. Our data are in agreement with those of Stein et al. (2011) (Table 1). The negative $\delta^{13}C$ excursion can be explained by the addition of relatively light carbon to the atmosphere and oceans; this could indicate episodes of intensified volcanic activity associated with the formation of the Ontong-Java Plateau, as has already been proposed for the negative excursion near the base of the Selli Level (Weissert and Erba, 2004; Mehay et al., 2009; Tejada et al., 2009; Erba et al., 2016). The stepwise increase in $\delta^{13}C$ values during stages C4–C6 occurs at a stratigraphic thickness of 1.67 m and lasted for approximately 1.02 Ma (Malinverno et al., 2012). This continuous positive shift is consistent with the reports of Li et al. (2008) and Hu et al. (2012) and may have been caused by periodic increases in organic carbon burial in the black shales during OAE1a (Menegatti et al., 1998; Kuhnt et al., 2011). The relatively stable values during the C7 stage occur at a stratigraphic level of 3.19 m (Figs. 4 and 5) and lasted for 0.75 Ma (Patruno et al., 2015). The duration of these high $\delta^{13}C$ values implies that mass and isotopic steady-state conditions were established. Assuming gradually decreasing primary productivity during the C7 stage, the extraction of ^{12}C into sedimentary carbon reservoirs would be balanced by the decreasing flux of isotopically light carbon into surface water reservoirs. Therefore, $\delta^{13}C$ values gradually decreased during the C8 stage to approach pre-excursion values, ranging from 3.85 to 2.47‰.

Table 1
Stratigraphic thicknesses and estimated durations of OAE1a, the transition interval and the C stages of the Gorgo a Cerbara section in central Italy (this study, Stein et al., 2011, and Patruno et al., 2015) with those of the Yenicesihlar section (Hu et al., 2012). Absolute ages follow the timescale of Malinverno et al. (2012).

Gorgo a Cerbara, Italy												Yenicesilar, Turkey				
Lithologic unit	Patruno et al. (2015)			This study				Stein et al. (2011)				Hu et al. (2012)				
	Lithozone	Thickness (m)	Duration (myr)	Thickness (m)		Carbon isotopic Stage	Duration (myr)	Thickness (m)		Carbon isotopic Stage	Duratio n (myr)	Thickness (m)		Carbon isotopic Stage	Duration (myr)	
ORB1	IX	13.33	4.1	13.15		C8–C9	4.2					3.4		C9		
	VIII	0.81	0.1													
Upper transition	VII	2.47	0.68	3.19		C7	0.75					20.34		C7–C8	1.3	
	VI	0.29	0.07													
OAE1a, Selli Level	V	1.9	1.11	1.81	0.93	C6	1.11	0.57	1.68	0.96	C6	0.63	2.1	0.52	C6	1.11	0.29
					0.63	C5		0.39		0.55	C5	0.36		0.4	C5		0.22
					0.11	C4		0.07		0.07	C4	0.05		0.6	C4		0.33
					0.14	C3		0.09		0.1	C3	0.07		0.58	C3		0.32
Lower transition	IV	0.26	0.033	0.34		C1–C2											
	III	0.58	0.207	5.53													
Maiolica	II	4.49	0.86														
	I	8.93	0.74														

These stable isotopic values and the C stages identified in the Gorgo a Cerbara section are similar to the results of Stein et al. (2011). They analyzed stable isotopic values and identified the C stages in the same section, but only focused on the record up to the OAE1a black shales; they did not evaluate the changes after OAE1a, especially during the transition from OAE1a to ORB1 (Fig. 9). In general, the record presented in our study is consistent with the previously mentioned records from Cismon (Menegatti et al., 1998), Sicily (Bellanca et al., 2002), La Bédoule (Herrle et al., 2004; Kuhnt et al., 2011), and Yenicesihlar (Hu et al., 2012) (Fig. 9). The major difference between the Gorgo a Cerbara section and these sections is the duration of the transition from OAE1a to ORB1. The transition interval spans approximately 3.19 m in the Gorgo a Cerbara section, lasting for 0.75 Ma and corresponding to carbon isotope stage C7 in the chemostratigraphy (Figs. 4 and 5). In contrast, the transition interval from OAE1a to ORB1 in the Yenicesihlar section (Hu et al., 2012) is approximately 20.34 m thick, lasting for approximately 1.3 Ma and corresponding to stages C7 and C8 (Fig. 9). If the end of the deposition of the Selli Level was synchronous around the globe, then the onset of ORB1 deposition was not isochronous, at least between the Yenicesihlar and Gorgo a Cerbara sections. Our results show that deposition of ORB1 in the Gorgo a Cerbara section occurred 0.55 Ma earlier than deposition of the Yenicesihlar section (Hu et al., 2012). This difference suggests that, from a carbon isotopic perspective, the system required different amounts of time to recover to the state that existed prior to the C3 perturbation.

6.3. Chronostratigraphy of the early Aptian paleoceanographic events

Combined stratigraphic, sedimentological, micropaleontological, and geochemical data allows us to construct a sequence of events during the late Barremian-early Aptian interval of the Gorgo a Cerbara section that includes the nannoconid crisis, negative $\delta^{13}C$ excursions, black-shale deposition and $CaCO_3$ dissolution associated with OAE1a (Fig. 10).

The nannoconid crisis is the most dramatic change in marine biota associated with OAE1a. It occurs just prior to the Selli Level interval and corresponds to the Lower Critical Interval of Coccioni et al. (2006) and lithozone IV of Patruno et al. (2015) in the Gorgo a Cerbara section (Fig. 10). It has been widely documented in the Tethyan realm, Boreal realm, as well as in the Atlantic and Pacific oceans (Menegatti et al., 1998; Channell et al., 2000; Bellanca et al., 2002; Erba and Tremolada, 2004; Erba et al., 2016). Our results allow a more precise placement of this event at the top of the C2 chemostratigraphic segment (Figs. 4 and 5), as has also been reported by Erba et al. (1999). According to the chronostratigraphic studies of Patruno et al. (2015), the late C2 interval, which includes the onset of the nannoconid crisis, corresponds to an interval between 120.793 and 120.76 Ma (i.e., the onset of the Selli Level). The diversification of new coccolith taxa and the biocalcification crisis of the heavily calcified nannoconids may be linked to rapidly rising CO_2 derived from the Ontong Java Plateau emplacement (Erba, 2004; Tejada et al., 2009; Patruno et al., 2015; Erba et al., 2016).

The negative $\delta^{13}C$ excursion occurs at 0.34 m in the Gorgo a Cerbara section (Fig. 10) just below the base of the Selli Level, was assigned to stage C3 by Menegatti et al. (1998). The excursion is concurrent with an abrupt increase in magnetic susceptibility values and a decrease in $CaCO_3$ content (Fig. 4). Following the timescale of Malinverno et al. (2012) and the reports of Patruno et al. (2015), the carbon isotope excursion (i.e., the Selli Level event) occurred at 120.76 Ma concurrent with the initiation of black-shale deposition and carbonate dissolution. Both calcareous nannofossils and planktic foraminifera are rare to absent and poorly preserved during the C3 interval with the exception of a temporary increase shortly after the beginning of OAE1a, as corroborated by bulk rock $CaCO_3$ content. Within the core of the Selli Level (0.59–1.97 m), a massive carbonate dissolution phase is observed as a result of excess CO_2, ocean acidification, and CCD shoaling (Malinverno et al., 2010). This acidification occurred 0.15 Ma after the beginning of OAE1a and lasted for 0.84 Ma assuming that the mean duration of OAE1a is 1.11 Ma. The acidification is evidenced by the absence or rarity of calcareous nannofossils in sediments (Leckie et al., 2002; Patruno et al., 2015). The lysocline then rapidly deepened during the final phase of stage C6, as suggested by the increase in $CaCO_3$ and the presence of calcareous plankton (Patruno et al., 2015). Rapid and massive carbon inputs has been shown to result from such an oscillation of the lysocline in carbon cycle models that include a weathering feedback. Massive black-shale deposition occurred at the base of the C6 stage and lasted for 0.4 Ma, which is corroborated by TOC and $\delta^{13}C_{org}$ values (Fig. 4). Enhanced primary productivity and nutrient availability are the generally accepted explanation for organic carbon burial and preservation or black-shale deposition (Erba, 2004). These features can be corroborated by maxima in both the C_{org}/P_{tot} ratios and the concentration of redox-sensitive elements (Stein et al., 2011).

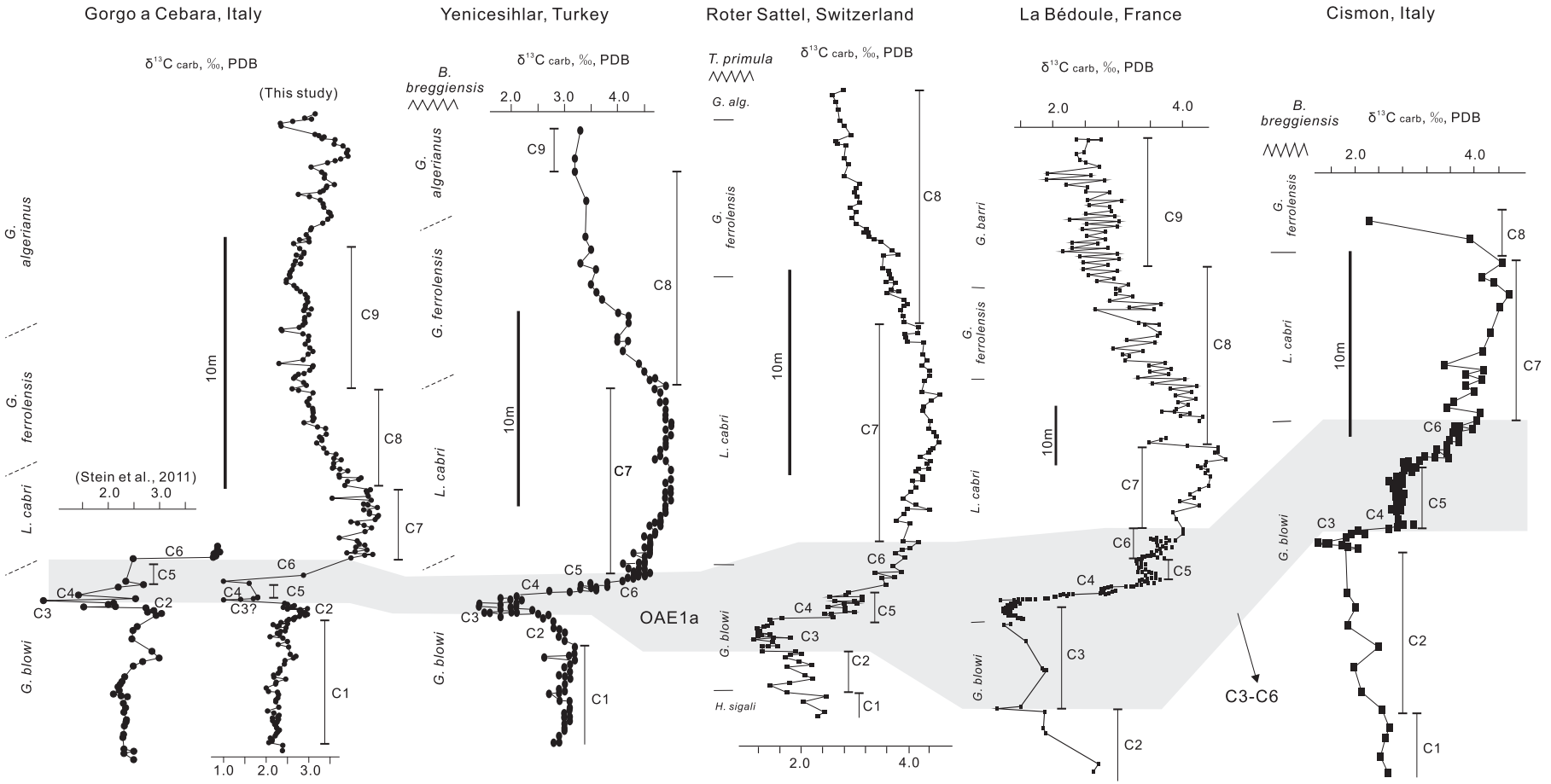

Fig. 9. Chemostratigraphic correlation of Aptian carbon stable isotopic values from the Gorgo a Cerbara section in central Italy (this study and Stein et al., 2011), the Yenicesihlar section (Hu et al., 2012), the Roter Sattel section in Switzerland (Menegatti et al., 1998), the La Bédoule section in France (Kuhnt et al., 2011), and the Cismon section in Italy (Menegatti et al., 1998).

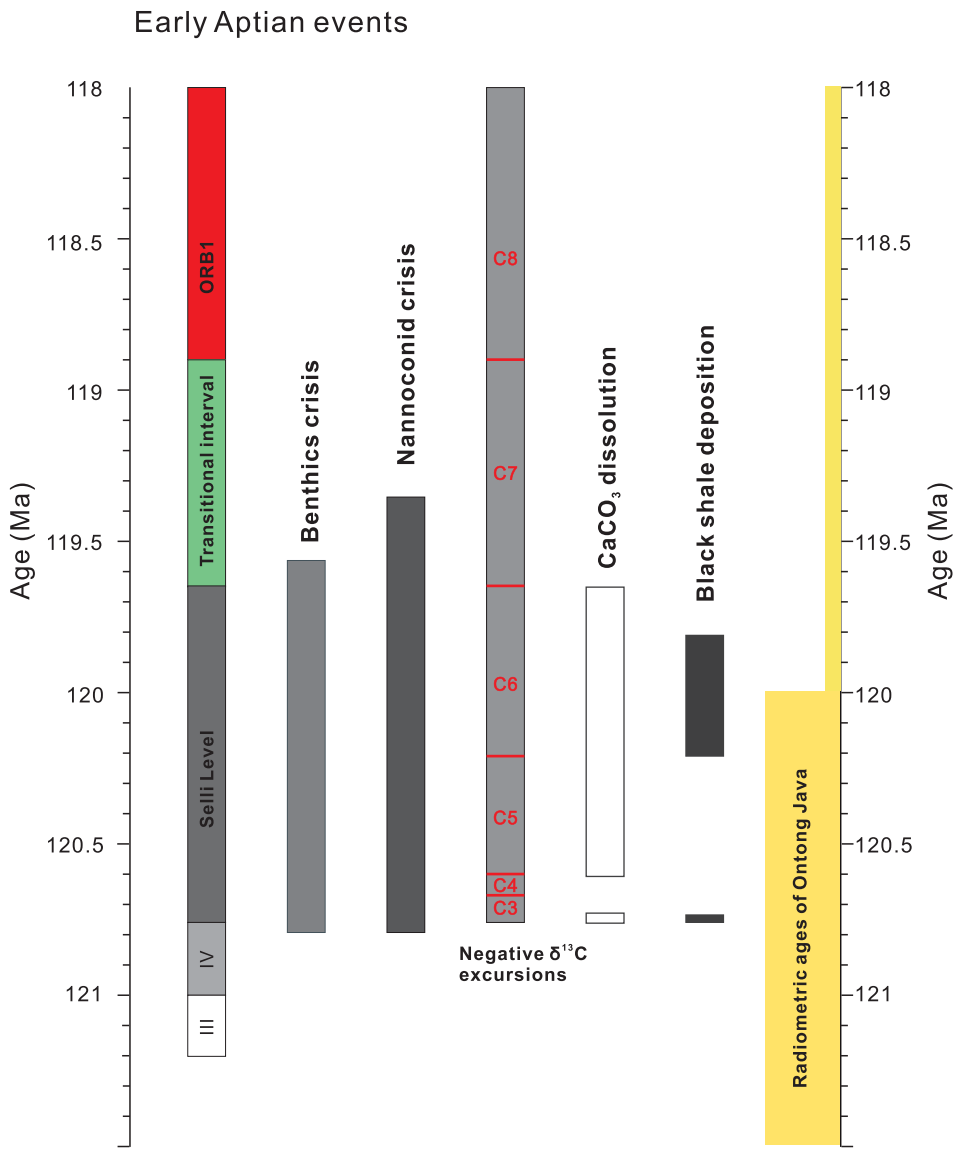

Fig. 10. Chronostratigraphy of early Aptian paleoceanographic events based on the results of this study and Patruno et al. (2015) for the Gorgo a Cerbara section. Absolute ages follow the timescale of Malinverno et al. (2012).

The increase in $\delta^{13}C$ values extends well above the Selli Level and lasted for 0.75 Ma, as documented by high $\delta^{13}C$ values during the C7 stage. This was concurrent with the return of both planktic foraminifera and various nanofloras and was followed by the deposition of dark red marlstones, red marly limestones and red calcareous shales (ORB1).

7. Conclusions

Combined stratigraphical, sedimentological, micropalaeontological and geochemical data allowed us to reconstruct in detail the paleoceanographic changes and chronostratigraphy from the OAE1a to the ORB1 during the Aptian.

1) OAE1a (the Selli Level) is approximately 1.81 m thick and consists of laminated to bioturbated olive gray, greenish gray and dark gray to black mudstones and shales. The black shales have high organic matter contents, with TOC values as high as 20.22%. The transition from OAE1a to ORB1 is approximately 3.19 m thick. It is lithologically characterized by bioturbated greenish gray cherty limestones and marly limestones with subordinate marls. ORB1 is over 13.15 m thick and is dominated by bioturbated strata, dark-red marlstones, red marly limestones and red calcareous shales with subordinate gray marlstones and marly limestones. The environment shifted from anoxic (during deposition of the OAE1a black shales) to oxic (during the transitional interval) and finally to highly oxic (during the ORB1 interval). The high organic carbon content and pyritization within the black shales of OAE1a suggest an anoxic environment. ORB1 represents a highly oxic environment, as shown by the hematite in the reddish limestones.
2) Carbon stable isotopic values from the bottom of OAE1a to the bottom of ORB1 shows several fluctuations, including a negative excursion (during stage C3, at 0.14 m) at the base of the Selli Level, a stepwise positive excursion (during stages C4 to C6, at 1.67 m) in the upper part of the Selli Level black shales and a positive carbon isotopic plateau (during stage C7, at 3.19 m) during the transitional interval. The stepwise positive shift may have been caused by periodic increases in organic carbon burial

in the black shales. The consistently high $\delta^{13}C_{carb}$ values during the C7 stage suggest that mass and isotopic steady-state conditions were established.

3) The transition interval from OAE1a to ORB1 lasts for 0.75 Ma in the Gorge a Cerbara section of Italy while it lasted for approximately 1.3 Ma in the Yenicesihlar section of Turkey. If the end of the deposition of the Selli Level was synchronous, then the onset of ORB1 deposition was not isochronous, indicating that, from a carbon isotopic perspective, the system required different amounts of time to recover to the state that existed prior to the stable carbon perturbation.
4) The nannoconid crisis occurred at the top of the C2 stage, just 0.34 m below the negative excursion in $\delta^{13}C$ isotopic values. The massive $CaCO_3$ dissolution phase associated with OAE1a occurs 0.25 m above the negative excursion in $\delta^{13}C$ isotopic values. It lasted for 0.85 Ma as a result of excess CO_2, ocean acidification, and CCD shoaling. Massive black shale deposition occurred at the base of the C6 stage and lasted for 0.4 Ma.

Acknowledgments

We thank Prof. R. Coccioni for inviting us to Italy for fieldwork and Zhong Han and Yongxiang Li for help with laboratory work. We are grateful to Dr. Stefano Patruno for providing us with his stratigraphic column. We also thank Dr. Stefano Patruno, Prof. Dr. Peter Harries and an anonymous reviewer for their constructive comments and suggestions. This study was financially supported by the Chinese MOST 973 Project (2012CB822001) and NSFC Project (41302033). This is a contribution to IGCP 609.

References

Arthur, M.A., Jenkyns, H.C., Brumsack, H.J., Schlanger, S.O., 1990. Stratigraphy, geochemistry, and paleoceanography of organic-carbon rich Cretaceous sequences. In: Ginsburg, R.N., Beaudoin, B. (Eds.), Cretaceous Research. Events and Rhythms Kluwer Acad, Norwell, pp. 75–119.

Baudin, F.Ë., Fiet, N., Coccioni, R., Galeotti, S., 1998. Organic matter characterisation of the Selli Level (Umbria-Marche Basin, central Italy). Cretaceous Research 19, 701–714.

Bellanca, A., Erba, E., Neri, R., Premoli Silica, I., Sprovieri, M., Tremolaca, F., Verga, D., 2002. Palaeoceanographic significance of the Tethyan 'Livello Selli' (early Aptian) from the Hybla Formation, northwestern Sicily: biostratigraphy and high-resolution chemostratigraphic records. Palaeogeography, Palaeoclimatology, Palaeoecology 185, 175–196.

Bottini, C., Cohen, A.S., Erba, E., Jenkyns, H.C., Coe, A.L., 2012. Osmium-isotope evidence for volcanism, weathering and ocean mixing during the early Aptian OAE 1a. Geology 40, 584–586.

Cai, Y., Hu, X., Li, X., Pan, Y., 2012. Origin of the red colour in a red limestone from the Vispi Quarry section (central Italy): a high-resolution transmission electron microscopy analysis. Cretaceous Research 38, 97–102.

Centamore, E., Fumanti, F., Nisio, S., 2002. The central-Northern Apennines geological evolution from Triassic to Neogene time. Bulletin de la Société Géologique, Italy 1, 181–197.

Channell, J.E.T., Erba, E., Muttoni, G.T.F., 2000. Early Cretaceous magnetic stratigraphy in the APTICORE drill core and adjacent outcrop at Cismon (Southern Alps, Italy), and correlation to the proposed Barremian-Aptian boundary stratotype. Geological Society of America Bulletin 112, 1430–1443.

Coccioni, R., Erba, E., Premoli-Silva, I., 1992. Barremian-Aptian calcareous plankton biostratigraphy from the Gorgo a Cerbara section (Marche, central Italy) and implication for plankton evolution. Cretaceous Research 13, 457–467.

Coccioni, R., Luciani, V., Marsili, A., 2006. Cretaceous oceanic anoxic events and radially elongated chambered planktic foraminifera: paleoecological and paleoceanographic implications. Palaeogeography, Palaeoclimatology, Palaeoecology 235, 66–92.

Coccioni, R., Jovane, L., Bancalà, B., Carla, F., Gerson, F., Fabrizio, J., Liliane, S., Jairo, P.d.A., Renato, L.M., Grasiane, R.I.F.d.T., 2012. Umbria-Marche Basin, Central Italy: a reference section for the Aptian-Albian interval at low latitudes. Scientific Drilling 13, 42–46.

Danelian, T., Baudin, F., Gardin, S., Beltran, C., Masure, E., 2002. Early Aptian productivity increase as recorded in the Fourcade level of the Ionian zone of Greece. Comptes Rendus Geoscience 334, 1087–1093.

Deaton, B.C., Balsam, W.L., 1991. Visible spectroscopyda rapid method for determining hematite and goethite concentration in geological materials. Journal of Sedimentary Petrology 61, 628–632.

Dumitrescu, M., Brassell, S.C., Schouten, S., Hopmans, E.C., Damsté, J.S.S., 2006. Instability in tropical Pacific sea-surface temperatures during the early Aptian. Geology 34, 833.

Erba, E., 1994. Nannofossils and superplumes: the early Aptian "nannoconid crisis". Paleoceanography 9, 483–501.

Erba, E., 2004. Calcareous nannofossils and Mesozoic oceanic anoxic events. Marine Micropaleontology 52 (2004), 85–106.

Erba, E., Channell, J.E.T., Claps, M., Jones, C., Larson, R., Opdyke, B., Premoli Silva, I., Riva, A., Salvini, G., Torricelli, S., 1999. Integrated stratigraphy of the Cismon APTICORE (Southern Alps, Italy): a "reference section" for the Barremian–Aptian interval at low latitudes. Journal of Foraminiferal Research 39, 371–391.

Erba, E., Tremolada, F., 2004. Nannofossil carbonate fluxes during the Early Cretaceous: phytoplankton response to nutrification episodes, atmospheric CO_2, and anoxia. Paleoceanography 19 (1).

Erba, E., Bottini, C., Weissert, H.J., Keller, C.E., 2010. Calcareous Nannoplankton response to surface-water Acidification Around Oceanic Anoxic Event 1a. Science 329, 428–432.

Erba, E., Duncan, R.A., Bottini, C., Tiraboschi, D., Weissert, H., Jenkyns, H.C., Malinverno, A., 2016. Environmental Consequences of Ontong Java Plateau and Kerguelen Plateau Volcanism, 30 GSA Special Paper.

Föllmi, K.B., Godet, A., Bodin, S., Linder, P., 2006. Interactions between environmental change and shallow-water carbonate build-up along the northern Tethyan margin and their impact on the early Cretaceous carbon-isotope record. Paleoceanography 21. http://dx.doi.org/10.1029/2006PA001313.

Ghirardi, J., Deconinck, J.-F., Pellenard, P., Martinez, M., Bruneau, L., Amiotte-Suchet, P., Pucéat, E., 2014. Multi-proxy orbital chronology in the aftermath of the Aptian Oceanic Anoxic Event 1a: Palaeoceanographic implications (Serre Chaitieu section, Vocontian Basin, SE France). Newsletters on Stratigraphy 47/3, 247–262.

Gradstein, F., Ogg, J., Schmitz, M., Ogg, G., 2012. The Geological Time Scale.

Herrle, J.O., Kößler, P., Friedrich, O., Erlenkeuser, H., Hemleben, C., 2004. High resolution carbon isotope records of the Aptian to Lower Albian from SE France and the Mazagan Plateau (DSDP Site 545): a stratigraphic tool for paleoceanographic and paleobiologic reconstruction. Earth and Planetary Science Letters 218 (1–2), 149–161.

Herbert, T.D., Premoli Silva, I., Erba, E., Fischer, A.G., 1995. Orbital chronology of Cretaceous–Paleocene marine sediments. In: Berggren, W.A., Kent, D.V., Aubry, M.-P., Hardenbol, J. (Eds.), Geochronology, Time Scale and Global Stratigraphic Correlation Society for Sedimentary Geology, Special Publication, 54, pp. 81–93.

Hu, X., Jansa, L., Sarti, M., 2006. Mid-Cretaceous oceanic red beds in the Umbria–Marche Basin, central Italy: constraints on paleoceanography and paleoclimate. Palaeogeography, Palaeoclimatology, Palaeoecology 233, 163–186.

Hu, X.M., Cheng, W.B., Ji, J.F., 2009. Origin of Cretaceous oceanic red beds from the Vispi Quarry section, central Italy: visible reflectance and inorganic geochemistry. In: Hu, X.M., Wang, C.S., Scott, R.W., Wagreich, M., Jansa, L. (Eds.), Cretaceous Oceanic Red Beds: Stratigraphy, Composition, Origins and Paleoceanographic and Paleoclimatic Significance, SEPM Special Publication, 91, pp. 183–197.

Hu, X., Zhao, K., Yilmaz, I.O., Li, Y., 2012. Stratigraphic transition and palaeoenvironmental changes from the Aptian Oceanic Anoxic Event 1a (OAE1a) to the oceanic red bed 1 (ORB1) in the Yenicesihlar section, central Turkey. Cretaceous Research 38, 40–51.

Jenkyns, H.C., 2003. Evidence for rapid climate change in the Mesozoic-Palaeogene greenhouse world. Philosophical Transactions of the Royal Society A 361, 1885–1916.

Ji, J.F., Balsam, W.L., Chen, J., Liu, L.W., 2002. Rapid and quantitative measurement of hematite and goethite in the Chinese loess-paleosol sequence by diffuse reflectance spectroscopy. Clays and Clay Minerals 50, 208–216.

Kuhnt, W., Holbourn, A., Moullade, M., 2011. Transient global cooling at the onset of early Aptian oceanic anoxic event (OAE) 1a. Geology 39, 323–326.

Leckie, R.M., Bralower, T.J., Cashman, R., 2002. Oceanic anoxic events and plankton evolution: biotic response to tectonic forcing during the mid-Cretaceous. Paleoceanography 17, 1–29.

Li, Y.X., Bralower, T.J., Montañez, I.P., Osleger, D.A., Arthur, M.A., Bice, D.M., Herbert, T.D., Erba, E., Premoli Silva, I., 2008. Toward an orbital chronology for the early Aptian Oceanic Anoxic Event (OAE1a, ~120 Ma). Earth and Planetary Science Letters 271, 88–100.

Marshall, J.D., 1992. Climatic and oceanographic isotopic signals from the carbonate rock record and their preservation. Geologic Magazine 129, 143–160.

Martinez, M., Pellenard, P., Deconinck, J.-F., Monna, F., Riquier, L., Boulila, S., Moiroud, M., Company, M., 2012. An orbital floating time scale of the Hauterivian/Barremian GSSP from a magnetic susceptibility signal (Río Argos, Spain). Cretaceous Research 36, 106–115.

Mehay, S., Keller, C.E., Bernasconi, S.M., Weissert, H., Erba, E., Bottini, C., Hochuli, P.A., 2009. A volcanic CO2 pulse triggered the Cretaceous Oceanic Anoxic Event 1a and a biocalcification crisis. Geology 37, 819–822.

Menegatti, A.P., Weissea, H., Brown, R.S., Tyson, R.V., Farrimond, P.a., Strasser, A., Caron, M., 1998. High-resolution C stratigraphy through the Early Aptian Livello Selli of the Alpine Tethys. Paleoceanography 13, 530–545.

Malinverno, A., Erba, E., Herbert, T., 2010. Orbital tuning as an inverse problem: chronology of the early Aptian oceanic anoxic event 1a (Selli Level) in the Cismon APTICORE. Paleoceanography 25, PA2203.

Malinverno, A., Hildebrandt, J., Tominaga, M., Channell, J.E.T., 2012. M-sequence geomagnetic polarity time scale (MHTC12) that steadies global spreading rates and incorporates astrochronology constraints. Journal of Geophysical Research: Solid Earth (1978–2012) 117 (B6).
Najarro, M., Rosales, I., Moreno-Bedmar, J.A., de Gea, G.A., Barrón, E., Company, M., Delanoy, G., 2011. High-resolution chemo- and biostratigraphic records of the Early Aptian oceanic anoxic event in Cantabria (N Spain): palaeoceanographic and palaeoclimatic implications. Palaeogeography, Palaeoclimatology, Palaeoecology 299, 137–158.
Patruno, S., Triantaphyllou, M.V., Erba, E., Dimiza, M.D., Bottini, C., Kaminski, M.A., 2015. The Barremian and Aptian stepwise development of the 'Oceanic Anoxic Event 1a' (OAE 1a) crisis: integrated benthic and planktic high-resolution palaeoecology along the Gorgo a Cerbara stratotype section (Umbria–Marche Basin, Italy). Palaeogeography, Palaeoclimatology, Palaeoecology 424, 147–182.
Schlanger, S.O., Jenkyns, H.C., 1976. Cretaceous oceanic anoxic events: causes and consequences. Netherlands Journal of Geosciences/Geologie en Mijnbouw 55 (3–4), 179–184.
Satolli, S., Besse, J., Speranza, F., Calamita, F., 2007. The 125–150 Ma high-resolution Apparent Polar Wander Path for Adria from magnetostratigraphic sections in Umbria–Marche (Northern Apennines, Italy): timing and duration of the global Jurassic–Cretaceous hairpin turn. Earth and Planetary Science Letters 257, 329–342.
Speranza, F., Satolli, S., Mattioli, E., Calamita, F., 2005. Magnetic stratigraphy of Kimmeridgian-Aptian sections from Umbria-Marche (Italy): new details on the M polarity sequence. Journal of Geophysical Research: Solid Earth 110, 1–26.
Stein, M., Föllmi, K.B., Westermann, S., Godet, A., Adatte, T., Matera, V., Fleitmann, D., Berner, Z., 2011. Progressive palaeoenvironmental change during the Late Barremian–Early Aptian as prelude to Oceanic Anoxic Event 1a: evidence from the Gorgo a Cerbara section (Umbria-Marche basin, central Italy). Palaeogeography, Palaeoclimatology, Palaeoecology 302, 396–406.
Tejada, M.L.G., Suzuki, K., Kuroda, J., Coccioni, R., Mahoney, J.J., Ohkouchi, N., Sakamoto, T., Tatsumi, Y., 2009. Ontong Java Plateau eruption as a trigger for the early Aptian oceanic anoxic event. Geology 37, 855–858.
Unida, S., Patruno, S., 2015. The palynostratigraphy of the upper Maiolica, Selli Level and the lower Marne a Fucoidi units in the proposed Barremian/Aptian (Lower Cretaceous) GSSP stratotype at Gorgo a Cerbara (Umbra-Marche Basin, Italy). Palynology 1–17. http://dx.doi.org/10.1080/01916122.2015.1029646.
Wagreich, M., Hu, X., Sageman, B., 2011. Causes of oxic–anoxic changes in Cretaceous marine environments and their implications for Earth systems-An introduction. Sedimentary Geology 235, 1–4.
Wang, C., Hu, X., Huang, Y., Wagreich, M., Scott, R., Hay, W., 2011. Cretaceous oceanic red beds as possible consequence of oceanic anoxic events. Sedimentary Geology 235, 27–37.
Weissert, H., Erba, E., 2004. Volcanism, CO_2 and palaeoclimate: a late Jurassic–early Cretaceous carbon and oxygen isotope record. Journal of the Geological Society, London 161, 695–702.

Appendix A. Supplementary data

Supplementary data related to this article can be found at http://dx.doi.org/10.1016/j.cretres.2016.04.016.